Design of a TE$_{34\ 10}$ mode cylindrical cavity for MW level gyrotron

MA Guo-Wu   HU Lin-Lin   ZHUO Ting-Ting   SUN Di-Min[*]   HUANG Yin-Hu
CHEN Hong-Bin   MENG Fan-Bao

(1. Institute of Applied Electronics China Academy of Engineering Physics Mianyang 621900 China)

Abstract: A cylindrical gyrotron cavity is designed and optimized with a high order mode TE$_{34\ 10-}$ to deliver an output power of megawatts level at 140 GHz. Analysis on mode competition indicates that the two adjacent modes TE$_{33\ 10-}$ and TE$_{31\ 11+}$ involve in competition and cause significant decreasing of output power of TE$_{34\ 10-}$. To suppress the competition hysteresis loops of TE$_{31\ 11+}$ and TE$_{33\ 10-}$ with TE$_{34\ 10-}$ are calculated which indicates TE$_{34\ 10-}$ can inhibit growth of the other two modes with decreasing magnetic field from its low efficiency single mode oscillation zone while it turned out just the opposite with increasing magnetic field due to the earlier oscillation of the competitors. Based on the results a multimode time-dependent calculation including 42 modes is carried out with magnetic field dropping from 5. 59 T to 5. 51 T the results show that mode competition is successfully suppressed the operation mode TE$_{34\ 10-}$ realizes stable single mode oscillation with an output power of 0. 96 MW and an electron efficiency of 36. 7% at 140 GHz.

Key words: gyrotron cylindrical cavities mode competition
PACS: 84. 40. Ik 84. 40. Fe 07. 57. Hm

MW   **TE$_{34\ 10}$**

*

(621900)

:   TE$_{34\ 10-}$ 140 GHz
.   TE$_{33\ 10-}$ TE$_{31\ 11+}$ TE$_{34\ 10-}$.

TE$_{34\ 10-}$

5. 59 T   5. 51 T   42
0. 96 MW

36. 7%   140 GHz.
:   ;   ;
: O46   : A

Introduction

Gyrotrons can produce hundreds of kilowatts or higher continuous-wave (CW) power in millimeter wave and higher frequency bands [1,2]. They have important applications in magnetically confined fusion such as plasma startup heating current driving and diagnostics [3-6]. To handle an output power of MW level the operating mode order should be increased as high as possible to minimize the heat density on the cavity wall but the mode competition deteriorates rapidly which restricts the further increasing of the mode order. In gyrotrons with cylindrical cavities which have realized MW level

output power，high order modes such as TE$_{25\ 10}$[7]，TE$_{28\ 8}$[8]，TE$_{31\ 8}$[9] and TE$_{31\ 11}$[10] have been successfully used and achieved continuous operation time of hundreds of seconds，while higher order modes such as TE$_{31\ 12}$[11]，TE$_{34\ 10}$[12]，TE$_{32\ 18}$[13] and so on have been studied with numerical calculations or short-duration experiments to further reduce heat dissipation difficulty. However stable operation of the higher order modes is always threatened by the mode competition. In the modes mentioned above，TE$_{34\ 10}$ is a promising candidate for MW level long pulse gyrotrons. Cavity designs with TE$_{34\ 10}$ have been carried out with PIC simulations in Ref. 12，and with a multimode time-dependent code named SELFT in Ref. 14，which show the TE$_{34\ 10}$ cavity have sufficient power capacity and acceptable efficiency for long pulse gyrotrons around 170 GHz.

In this paper，a cylindrical TE$_{34\ 10}$ cavity is designed with an in-house developed code GYO. We mainly focus on the possible competitors to the TE$_{34\ 10}$ mode and try to avoid the interference in the steady operation. A time-varying magnetic field is introduced into the starting process to realize single mode stable oscillation. The RF losses in the cavity is calculated，which is far less than the critical value. The structure of the article is organized as below: the first part briefly reviews the theoretical models used in GYO，which consists of LN-module for linear theoretical calculation，SSC-module for single-mode self-consistent theoretical calculations，and MTC-module for multimode time-dependent theoretical calculations. The second part presents the design of the cavity and suppression of competition modes. In the third part the loss power density on the cavity wall is obtained. Conclusion will be given in the end.

1 Theoretical model

The theoretical models used in GYO consist of the linear theory，the nonlinear self-consistent theory and the multimode time-dependent theory，which correspond to the LN module，SSC module and MTC module. The linear theory is always used to obtain the oscillation starting conditions，and the nonlinear self-consistent theory represents the stationary interaction of a single mode and the beam，which could be used to optimize the parameters. The multimode time-dependent theory can include several modes in the calculation and acquire multimode interaction state in time domain，which is helpful in analysis of mode competition.

One of the most important parameters derived from the linear theory is the threshold current，which could be described as[15]

$$
-1/I_{st} = \left(\frac{Q Z_0 \eta}{8 \gamma_0 c^2} \right) \left(\frac{\pi}{\lambda} \int_0^L |f(z)|^2 dz \right)^{-1}
$$

$$
\cdot \left(\frac{k_{mn} C_{mn} C_{mn}}{\beta_{z0}(s-1)!} \right)^2 \left(\frac{c k_{mn} \gamma_0 \beta_{\perp 0}}{2\Omega_0} \right)^{2(s-1)}
$$

$$
\cdot \left(s + \frac{1}{2} \frac{\omega \beta_{\perp 0}^2}{v_{z0}} \frac{\partial}{\partial \Delta_s} \right) \cdot \left| \int_0^L f(z) e^{i\Delta_s z} dz \right|^2
$$

(1)

where

$$
C_{mn} = \left[\sqrt{\pi(x_{mn}^2 - m^2)} J_m(x_{mn}) \right]^{-1} \quad (2)
$$

$$
G_{mn} = J_{m \mp s}(k_{mn} R_e) \quad (3)
$$

where $f = |f| \exp(-i\psi(z))$ is field profile function，Q is quality factor of the cavity，Z_0 is wave impedance in vacuum，η is charge-mass ratio，s is the harmonic number，$m - +s$ corresponds to the case of azimuthal co-rotation and counter-rotation of the wave and the electron，$\beta_{\perp 0}$ is transverse velocity and β_{z0} is axial velocity of electrons normalized by light speed c respectively，$k_\perp$ is transverse wave number，R_e is injection radius of the beam，$\Delta_s(z)$ is the mode detuning parameter given by

$$
\Delta_s(z) = \frac{\omega}{v_{z0}} \left(1 - \frac{s\Omega_0}{\omega \gamma_0} \right) \quad (4)
$$

where ω is frequency of wave and $\Omega_0 = eB/m_0$ is non-relativistic cyclotron frequency of electron. The coupling coefficient represents the coupling strength between electron beam and specific mode，and could be described by[16]

$$
C_{BF} = \frac{J_{m \pm s}^2(k_\perp R_e)}{(x_{mn}^2 - m^2) J_m^2(x_{mn})} \quad . \quad (5)
$$

Equation (5) indicates the strongest coupling occurs at the first maximum of $J_{m-s}(k_\perp R_e)$ which is also the first zero of $J'_{m-s}(k_\perp R_e)$.

The nonlinear self-consistent theory is composed of the adiabatic equation for electron motion and the wave equation for the RF field profile function，which can be expressed respectively as[17]

$$
d/d\ell + (i\gamma/\gamma_0)(1/s - \bar\Omega_0/\gamma\bar\omega) \ P
$$
$$
= -(1/2\bar\omega)(\gamma/\gamma_0)(\bar k_{mn}/\bar\Omega_0)^{s-1}(J_{m-s}(\bar k_{mn}\bar R_0)/\bar r_w) F(P^{s-1})^* \quad (6)
$$

and

$$
d^2/d\ell^2 + \beta_{z0}^2(1 - \bar k_{mn}^2/\bar\omega^2) \ F
$$
$$
= -(i\mu\eta/c)\beta_{z0}(I_0/\gamma_0\bar\omega) \ x_{mn}C_{mn}/2^{s-1}(s-1)!^2(\bar k_{mn}/\bar\Omega_0)^{s-1}
$$
$$
\times \ J_{m-s}(\bar k_{mn}\bar R_0)/\bar r_w \ (1/2\pi)\int_0^{2\pi} d\Lambda_0 P^s \quad (7)
$$

where $P = \bar u_t \exp(-i\Lambda)$ is normalized momentum variable，$\bar u_t = \gamma v_t/c$ is the normalized transverse momentum，$\beta_{z0} = v_{z0}/c$ is normalized initial axial velocity，$\Lambda = (\underline{\omega}/s - \Omega)\tau + \omega/st_0 - \phi$ is slow time phase variable，$\bar\Omega = \Omega r_{w0}/c = \Omega_0 r_{w0}/\gamma_0 c$ is normalized cyclotron frequency of the electron，r_{w0} is an arbitrary radius for normalization，t_0 is the moment when electrons enter the cavity，$\tau = t - t_0$，φ is the polar angle of guiding center，$F = C_{mn}X_{mn}\eta f/c^2 2^{s-1}!$ is normalized field profile function，$C_{mn} = \{\sqrt{\pi(x_{mn}^2 - m^2)} \ J_m(x_{mn})\}^{-1}$ is a normalization constant，$\bar r_w = r_w/r_{w0}$ is normalized wave guide radius，$\bar R_e = R_e/r_w$ is normalized injection radius，$\bar k_{mn} = k_{mn}/r_{w0}$ is normalized transverse wave number，$\ell = \omega z/v_{z0} = \omega(t - t_0)$ is normalized z coordinate of the electron.

The multimode time-dependent theory could be derived from the nonlinear self-consistent theory based on the fact that characteristic rise time of fields in the resonator is much longer than the electron transit time in the cavity as well as the wave period，which are given by[18]

$$
\frac{da_n}{dt} + \frac{\omega_0 a_n}{2Q_n} = \frac{-1}{2\varepsilon_0} \mathrm{Im}\mathfrak{R}_n(t) \quad (8)
$$

and

$$\frac{\mathrm{d}\psi_n}{\mathrm{d}t} + \omega_0 - \omega_n = \frac{1}{2\varepsilon_0 a_n}\mathrm{Re}\Re_n(t) \qquad (9)$$

where $a_n(t)$ is amplitude and ψ_n is phase of the field ω_n is a nearby reference frequency ε_0 is permittivity of free space $\Re_n(t) = i\int_V \mathrm{d}a\mathrm{d}zf(z)\ \overrightarrow{e}_n^* \cdot \overrightarrow{J}_\omega e^{i\psi}/W$ is the complex slow-time-scale component of the electron-beam polarization $\overrightarrow{e}_n^*$ is the waveguide transverse-mode vector function $\overrightarrow{J}_\omega = \int_0^{2\pi} d(\omega_0 t) \overrightarrow{J}_t e^{i\omega_0 t}$ is the rf current density $\overrightarrow{J}_t$ is the transverse current density of the beam $W = \int_0^L \mathrm{d}z \mid f(z)\mid^2$. The definition of other variables in (8) and (9) is the same as in (6) and (7) except the subscript identifies the mode n.

2   Design of the cavity and realization of single-mode steady operation

A simple three-segment structure including down taper uniform section and up taper is adopted in the cavity. The length of the uniform section is expressed as L and the radius of the uniform section is R_0. R_0 is set as 25. 45 mm according to the cutoff frequency of the waveguide. The cavity structure and field distribution under different L are shown in Fig. 1(a). The resonant frequency and the Q-factor of the cavity are shown in Fig. 1(b).
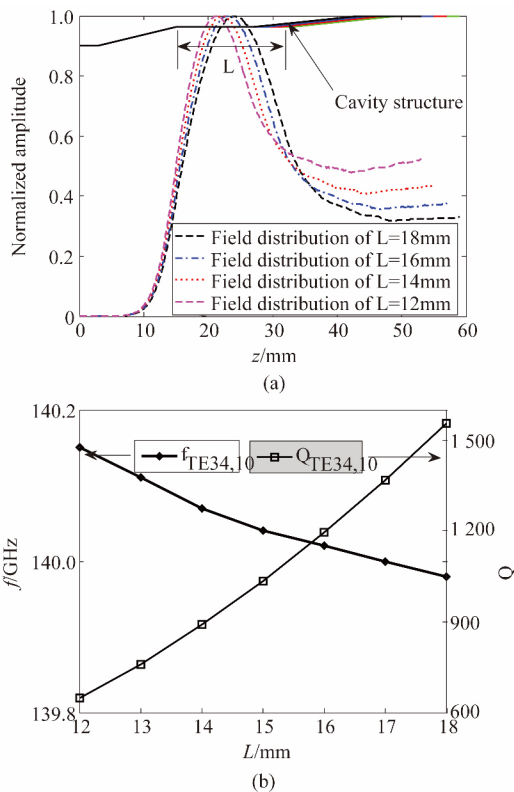

Fig. 1   (a) Cavity structure and field distribution (b) resonant frequency and Q factor of the cavity
图 1   (a) 腔体结构和场分布   (b)   谐振频率和 Q 值

We choose co-rotation of the wave and the beam for better beam-wave interaction which means the operation mode is TE$_{34\ 10-}$. With beam voltage 75 kV beam current 35 A pitch factor 1. 5 and injection radius 12. 16 mm the output power of the cavity is calculated with SSC module the results are shown in Fig. 2. As shown in the figure the output power rises with L but the growth rate slows down when it reaches 16 mm. Although longer cavity length can increase output power slightly it will bring the risk of deterioration of mode competition so we choose L to be 16 mm the maximum output power could reach 1. 1 MW at magnetic field of 5. 52 T with an efficiency of 41. 9%.
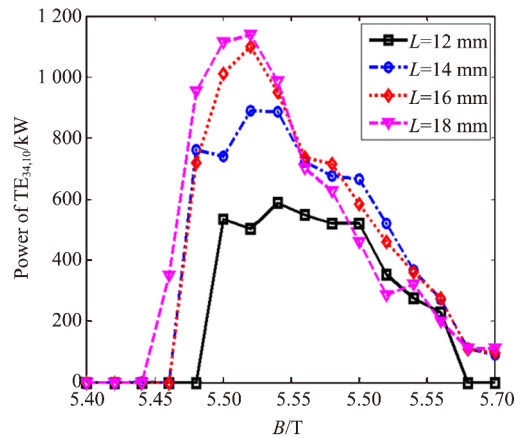

Fig. 2   Output power versus magnetic field under different L calculated by SSC module
图 2   不同 L 下由 SSC 模块计算的输出功率随磁场的变化

Now we consider the modes which might participate in competition with operation mode TE$_{34\ 10}$. The coupling coefficients and corresponding eigenvalues of the nearby modes are plotted in Fig. 3(a) in which TE$_{31\ 11+}$ and TE$_{33\ 10-}$ have the coupling coefficient similar to TE$_{34\ 10-}$. The threshold currents of the modes are plotted in Fig. 3(b) we can see that many of the neighbor modes have starting current below 35 A and therefore are capable of oscillating so the process of starting oscillation is also a process of competition among these modes.

The MTC module is used to study the starting process of the oscillation 13 modes thought to be most dangerous are included according to Fig. 3(a) and fixed static magnetic field is adopted. The results are counted in Fig. 4(a) which shows that TE$_{34\ 10-}$ can only achieve stable oscillation between 5. 57 T and 5. 68 T but fails at magnetic field between 5. 44 T and 5. 56 T where TE$_{33\ 10-}$ or TE$_{31\ 11+}$ dominates the oscillation. The results of SSC calculation of the three modes are also given in Fig. 4(a) which expect an output power of 1. 1 MW for TE$_{34\ 10-}$ but only 664 kW could be achieved according to the MTC calculation due to the competition of TE$_{33\ 10-}$ and TE$_{31\ 11+}$.

Fig. 4(b) shows the time behavior of the modes with a fixed magnetic field of 5. 55 T the initial power of each mode is set to be 0. 1 kW. The power of TE$_{28\ 12-}$
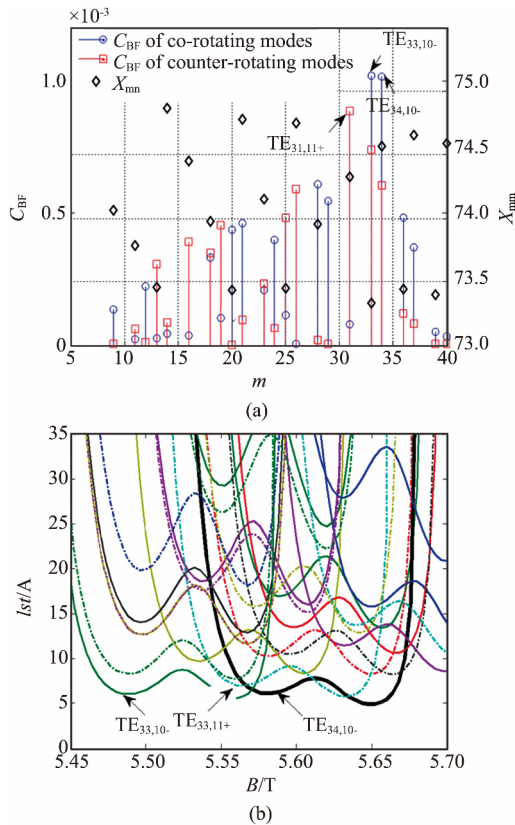
(a)

(b)

Fig. 3 (a) Coupling coefficient of co‑rotating modes (blue circles) and counter‑rotating modes (red squares) together with the eigenvalues of the modes (black diamonds). (b) Threshold current curves of co‑rotating modes (solid lines) and counter‑rotating modes (dashed lines) whose eigenvalues are close to $TE_{34\ 10}$

3 (a)   (
)   (   )
(   );(b) $TE_{34\ 10}$
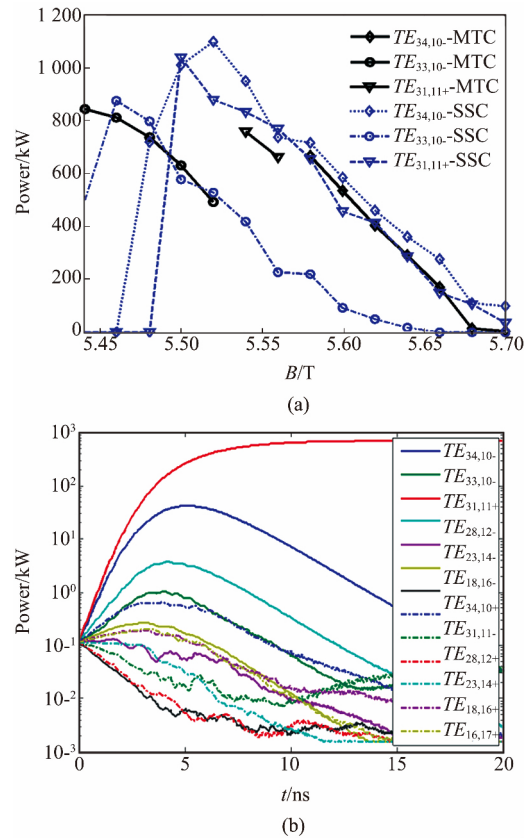   (   )   (   )

(a)

(b)

Fig. 4 (a) Output power versus magnetic field calcu‑lated by SSC (blue dashed lines) and MTC (black sol‑id lines). (b) Output power of each mode versus time at B = 5.56 T

4 (a) SSC   (   ) MTC   (
)   ;(b) B = 5.56 T

$TE_{31\ 11+}$, $TE_{33\ 10-}$, $TE_{34\ 10-}$ and $TE_{34\ 10+}$ grow together in the beginning, while $TE_{31\ 11+}$ have the maximal growth. The output power of the other modes reaches the inflec‑tion point at about 5 ns, after the output power of $TE_{31\ 11+}$ grows to saturation, all the other modes are sup‑pressed and the system is dominated by $TE_{31\ 11+}$, the ex‑pected operation mode $TE_{34\ 10-}$ fails to achieve stationary oscillation finally.

The magnetic field we use in the calculations above is a fixed one, which doesn't seem to achieve an effi‑cient operation state for $TE_{34\ 10-}$ mode. From Fig. 4(a) we can see that $TE_{34\ 10-}$ can obtain stable oscillation at magnetic field between 5.57 T and 5.68 T, due to the inhibition effect of the preset field on the other mode, a time‑varying magnetic field which decreases after the op‑eration mode achieving stable oscillation might be helpful to improve the efficiency. To verify the feasibility of the method, it is necessary to obtain the hysteresis curves of $TE_{31\ 11+}$ and $TE_{33\ 10-}$ with $TE_{34\ 10-}$ first. The scanning range of the magnetic field is chosen to be 5.45 T ~ 5.59 T, the scanning process is that the magnetic field decrea‑ses from 5.59 T to 5.45 T at a uniform speed in 500 ns, then maintains 5.45 T for 100 ns, and then rises to 5.59 T again in 500 ns. The calculated hysteresis loop of $TE_{33\ 10-}$ and $TE_{34\ 10-}$ is shown in Fig. 5(a). As shown in the Fig. 5(a), $TE_{34\ 10-}$ starts oscillation first at $B = 5.59$ T while $TE_{33\ 10-}$ damps rapidly. In the process of mag‑netic field falling from 5.59 T, $TE_{34\ 10-}$ remains dominant and its output power increases gradually and reaches the maximum at about 5.5 T. After that, the output power of $TE_{34\ 10-}$ begins to decrease as the magnetic field decrea‑ses. When the magnetic field reaches 5.485 T, the dom‑inant mode is switched from $TE_{34\ 10-}$ to $TE_{33\ 10-}$. The out‑put power of $TE_{34\ 10-}$ decreases rapidly while $TE_{33\ 10-}$ rises to the peak. As the magnetic field continues to decrease, the power of $TE_{33\ 10-}$ is still rising until it reaches 5.45 T. After the retention time of 100 ns, the magnetic field be‑gins to increase, $TE_{33\ 10-}$ remains dominant until the mag‑netic field increases to 5.58 T where the oscillation mode is switched from $TE_{33\ 10-}$ to $TE_{34\ 10-}$ again. In the magnetic field area between 5.485 T and 5.58 T, both modes can achieve steady single‑mode oscillation, the dominant mode is determined by the changing direction of the mag‑netic field. Similar conclusion can also be obtained from

MA Guo-Wu *et al*: Design of a TE$_{34\ 10}$ mode cylindrical cavity for MW level gyrotron

the hysteresis loop between TE$_{31\ 11+}$ and TE$_{34\ 10-}$ as shown in Fig. 5(b). In fact the above phenomenon is caused by the inhibition effect of the mode which obtains a certain oscillation amplitude first on the other modes. So to realize a high-power output of TE$_{34\ 10-}$ we can start at arbitrary magnetic field between 5.57 T and 5.68 T where TE$_{34\ 10-}$ can retain single-mode steady oscillation and change the magnetic field to a more efficient point after the expected mode is excited.
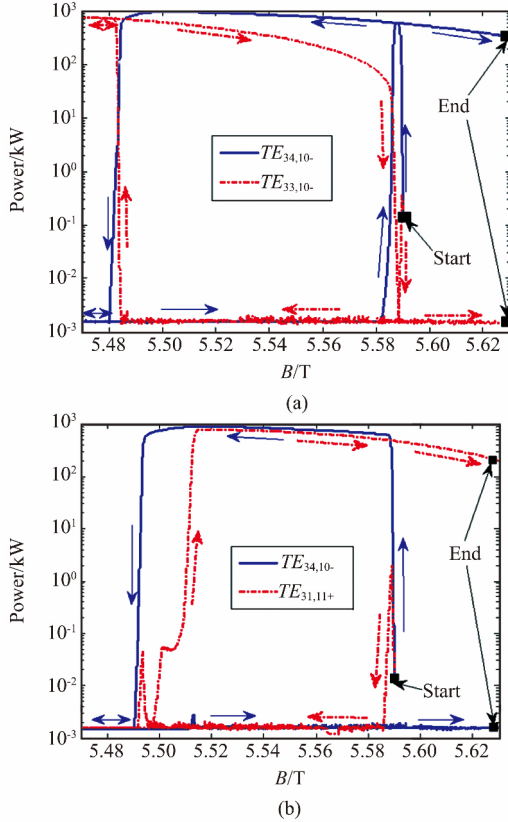

(a)

(b)

Fig. 5 (a) Hysteresis loop between TE$_{34\ 10-}$ and TE$_{33\ 10-}$ (b) Hysteresis loop between TE$_{34\ 10-}$ and TE$_{31\ 11+}$. The magnetic field varies as: decreasing from 5.59 T to 5.45 T in 500 ns then maintaining 5.45 T for 100 ns and then rising to 5.59 T again in 500 ns

5 (a) TE$_{34\ 10-}$ TE$_{33\ 10-}$; (b) TE$_{34\ 10-}$ and TE$_{31\ 11+}$. :

500 ns 5.59 T 5.45 T 5.45 T
100 ns 500 ns 5.59 T

The dependence of magnetic field on time we use finally is shown in Fig. 6 which also contains the corresponding MTC calculation results including 42 neighbor co-rotating and counter-rotating modes. From Fig. 6 we can see the magnetic field maintains 5.59 T for 5 ns during which the output power of TE$_{34\ 10-}$ increases to more than 100 kW while most of the other modes have negative growth rate except several modes growing with it and reaching their inflection point at about 4 ns. After that the magnetic field starts to decrease and the power of TE$_{34\ 10-}$ continues to grow. The system achieves single mode steady operation of TE$_{34\ 10-}$ at last with an output
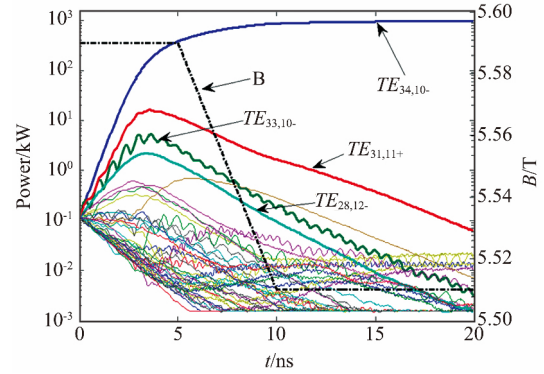

Fig. 6 MTC calculation results including 42 modes with time-varying magnetic field

6 42 MTC

power of 964 kW and an efficiency of 36.7% at magnetic field of 5.51 T. The mode competition is successfully suppressed and the power of all other modes is far less than 1 kW at the end of the calculation. The output power of TE$_{34\ 10-}$ is still smaller than the maximum 1.1 MW obtained by SSC calculation which may be caused by the influence of the other modes with small amplitudes on the interaction between the operation mode and the beam.

3 Ohmic wall loss

In the interaction cavity some amount of RF power is lost due to the ohmic wall loss which would heat the cavity and elevate the temperature of the wall. So cooling system is needed to keep the temperature within a certain range. To ensure feasible operation of the gyrotron a general limitation is set for the wall loading as 2 kW/cm^2 for CW operation [19]. The ohmic wall loss can be calculated as below [20]

$$\frac{\mathrm{d}P_{loss}}{\mathrm{d}A} \simeq \frac{\delta}{4\pi\mu_0\omega}\left[\frac{1}{x_{mn}^2-m^2}\right]\left(k_{mn}^4 \mid f \mid^2 + \frac{m^2}{r_w^2}\left|\frac{\mathrm{d}f}{\mathrm{d}z}\right|^2\right)$$

(10)

where $\delta=\sqrt{2/\mu_0\omega\sigma}$ is the skin depth μ_0 is the permittivity σ is the electrical conductivity. The other parameters are the same as before.

The wall loading of the cavity is calculated as in Fig. 7 the peak loss power density is about 0.67 kW/cm^2 with an output power of about 1 MW which is far less than the critical value. It makes the heat dissipation easier and is helpful to improve the stability and reliability of the gyrotron.

4 Conclusions

A cavity operating at TE$_{34\ 10-}$ is designed in the article. According to the analysis of eigenvalues and coupling coefficients of the neighbor modes TE$_{33\ 10-}$ and TE$_{31\ 11+}$ are more dangerous to the operation mode than the else which is verified by MTC calculations. Using the time-varying magnetic field method the mode compe-
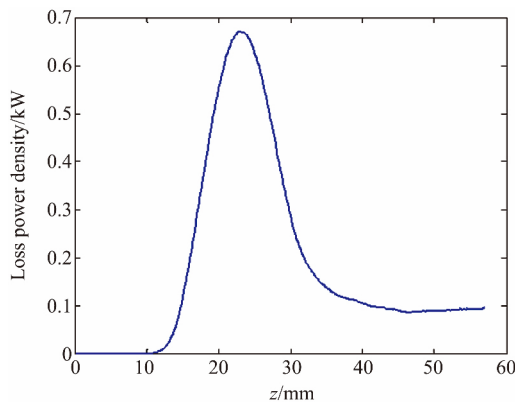
Fig. 7　Distribution of loss power density on the cavity wall

7

tition is suppressed and single-mode steady operation with an output power of 964 kW at 140 GHz is achieved. The peak ohmic wall loading of the cavity is only 0. 67 kW/cm^2 which is beneficial for cooling system design and achieving stable CW operation. Besides　according to our analysis　as long as we can make the expected mode start first　competitive inhibition can be achieved so adjustment methods based on other parameters may be also feasible　such as the beam voltage　pitch factor etc.

References

1　Nusinovich G S　Thumm M K A　Petelin M I. The Gyrotron at 50: Historical Overview　J　. *Journal of Infrared Millimeter & Terahertz Waves*　2014　**35**（4）: 325-381.

2　FU Wen-Jie　GUAN Xiao-Tong　CHEN Chi　et al. A 220GHz high-power coaxial cavity gyrotron　J　. *J. Infrared Millim. Waves*　（

．220 GHz　　　　　　　　　　　　　　．

）2014　**33**（6）: 613-618.

3　Gaponov A V　Flyagin V A　Goldenberg A L　et al. Powerful millime-tre-wave gyrotrons　J　. *International Journal of Electronics*　1981　**51**（4）: 277-302.

4　Thumm M. Progress on Gyrotrons for ITER and Future Thermonuclear Fusion Reactors　J　. *IEEE Transactions on Plasma Science*　2011　**39**（4）: 971-979.

5　Litvak A　Sakamoto K　Thumm M. Innovation on high-power long-pulse gyrotrons　J　. *Plasma Physics & Controlled Fusion*　2011　**53**（12）: 124002.

6　Poli E　Tardini G　Zohm H　et al. Electron-cyclotron-current-drive efficiency in DEMO plasmas　J　. *Nuclear Fusion*　2013　**53**（1）: 013011.

7　Litvak A G　Denisov G G　Myasnikov V E　et al. Recent Develop-ment Results in Russia of Megawatt Power Gyrotrons for Plasma Fusion Installations　C　// *EDP Sciences*　2012: 04003.

8　Thumm M　Alberti S　Arnold A　et al. EU Megawatt-Class 140-GHz CW Gyrotron　J　. *IEEE Transactions on Plasma Science*　2007　**35**（2）: 143-153.

9　Sakamoto K　Kasugai A　Kajiwara K　et al. Progress of high power 170 GHz gyrotron in JAEA　J　. *Nuclear Fusion*　2009　**49**（9）: 095019.

10　Ikeda R　Oda Y　Kobayashi T　et al. Development of 170 GHz 1 MW gyrotron with high-order TE 31 11　mode oscillation for ITER EC system　J　. *Fusion Engineering & Design*　2018　**128**: 23-27.

11　Kajiwara K　Oda Y　Takahashi K　et al. Design and Operation of TE 31 12 High Power Gyrotron　J　. *Fusion Science & Technology*　2013　**63**（1T）: 35-39.

12　Kumar A　Kumar N　Singh U　et al. Towards a 1 MW 170 GHz gy-rotron design for fusion application　J　. *Infrared Physics & Technolo-gy*　2013　**57**（3）: 1-7.

13　Sakamoto K　Kariya T　Oda Y　et al. Study of sub-terahertz high pow-er gyrotron for ECH&CD system of DEMO　C　// *IEEE International Conference on Plasma Sciences. IEEE*　2015: 1-1.

14　Kern S　Borie E　Illy S　et al. Theoretical study of 174 GHz operation of the W7-X 1 MW 140 GHz gyrotron　C　// *International Conference on Infrared Millimeter and Terahertz Waves*　California Institute of Technology Pasadena　California　USA　2008: 1-2.

15　Borie E　Jodicke B. Comments on the linear theory of the gyrotron　J　. *IEEE Transactions on Plasma Science*　2002　**16**（2）: 116-121.

16　Nusinovich G S. *Introduction to the Physics of Gyrotrons*　M　. Balti-more MD: John Hopkins University Press　2004　62.

17　Fliflet A W　Read M E　Chu K R　et al. A self-consistent field theory for gyrotron oscillators: application to a low Q gyromonotron　J　. *Inter-national Journal of Electronics*　1982　**53**（6）: 505-521.

18　Fliflet A W　Lee R C　Gold S H　et al. Time-dependent multimode simulation of gyrotron oscillators　J　. Physical Review A　1991　**43**（11）: 6166-6176.

19　Gantenbein G　Borie E　Dumbrajs O　*et al*. Design of a high order volume mode cavity for a l MW/140GHz gyrotron　J　. *International Journal of Electronics*　1995　**78**（4）: 771-787.

20　Jackson　J. D. *Classical Electrodynamics*　M　. New York: John Wiley & sons　Inc.　1962　36.